Vol 14 No 7, July 2005
1009-1963/2005/14(07)/1398-09

Chinese Physics

© 2005 Chin. Phys. Soc.
and IOP Publishing Ltd

A new lattice Boltzmann model for incompressible magnetohydrodynamics*

Chen Xing-Wang(陈兴旺) and Shi Bao-Chang(施保昌)†

Department of Mathematics, Huazhong University of Science and Technology, Wuhan 430074, China

(Received 13 September 2004; revised manuscript received 28 December 2004)

Most of the existing lattice Boltzmann magnetohydrodynamics (MHD) models can be viewed as compressible schemes to simulate incompressible MHD flows. The compressible effect might lead to some undesired errors in numerical simulations. In this paper a new incompressible lattice Boltzmann MHD model without compressible effect is presented for simulating incompressible MHD flows. Numerical simulations of the Hartmann flow are performed. We do numerous tests and make comparison with Dellar's model in detail. The numerical results are in good agreement with the analytical solutions. The scheme preserved a consistent approximation of the divergence-free condition $\nabla \cdot B = 0$ to round-off error.

Keywords: lattice Boltzmann method, MHD, incompressible
PACC: 4700, 5230, 0270

1. Introduction

During the last few years, the lattice Boltzmann method (LBM) has been successfully applied in simulation of fluid flows, such as hydrodynamic systems, magneto-hydrodynamic systems, multiphase and multi-component fluids including suspensions and emulsions, chemical-reactive flows, and multi-component flow through porous media. The LBM originated from a Boolean fluid model, the so-called lattice gas automata (LGA). Frisch, Hasslacher, and Pomeau (FHP) proposed the first LGA model[1] usually named FHP gas, which uses a hexagonal lattice with six particle speeds for simulating two-dimensional hydrodynamics. However, there are some shortcomings such as the lack of Galilean invariance and statistical noise with LGA model. Instead of following the dynamics of individual particles, lattice Boltzmann methods use the single-particle distribution function which is more efficient and accurate computationally and essentially noise-free.

The first magneto-hydrodynamic LGA was developed by Montgomery and Doolen[2,3] shortly after the FHP gas. Their model is an extension of the original FHP gas. It includes additional degrees of freedom of the particles for the vector potential, which has only one component in two dimensions and satisfies a passive scalar equation similar to the temperature. Therefore, the model is confined to two dimensions. Additionally, the model does not include the Lorentz force, which must be appended factitiously as an external force that needs some space averages when simulating.

Originally, only mass and momentum conservations were considered in the lattice Bathnagar–Gross–Krook (LBGK) method, which is the simplest and most popular lattice Boltzmann method. However, in many applications it is important and sometimes critical to consider the magnetic effects in fluid flows. LBGK models for magnetohydrodynamics (MHD) flows have been developed by several groups. In general, these lattice Boltzmann MHD models fall into two categories: the multi-speed (MS) approach and multi-distribution-function (MDF) approach. The MS approach is a straightforward extension of the lattice Boltzmann models[4−6] presented by Martinez, Chen and Matthaeus in which a tensor (i.e., two-indexed) particle representation and a bi-directional streaming mechanism are used. For each one of these particles, there are two vectors attached, representing the momentum and magnetic field. These MS models in-

*Project supported by the National Natural Science Foundation of China (Grant Nos 70271069 and 60073044).
†Corresponding author. E-mail: sbchust0382@sina.com

troduce some additional discrete velocities and the equilibrium distributions usually include higher order velocity terms. However, this model is confined to low-Reynolds because the values of the transport coefficients at the stability threshold are finite and its extension to three dimensions would require a large amount of computational memory. Such limitations severely restrict the MDF model's applications.

However, the limitations of the MS approach can be partly overcome by the MDF approach. In the MDF model[7] presented by Dellar, the Lorentz force can be introduced as a point-wise force, the induction equation is also solved using an LBGK equation by introducing an independent distribution function. MDF models can improve the numerical stability. The accuracy of the MDF models has been verified by several benchmark studies in Refs.[8,9]. Despite the advantage of the MDF models, there are still some limitations. For instance, in order to get the correct macroscopic equation from the MDF models, it must be assumed that the Mach number of the flow is small and the density varies slowly. When used for incompressible flows, the method must be viewed as an artificial compressible method. In some cases, such as turbulent flows, this compressibility may produce some undesired nonphysical phenomena. Some efforts have been made to reduce or eliminate such errors for lattice Boltzmann MHD models. Recently, Macnab *et al* presented another octagonal lattice Boltzmann MHD model,[10] which possesses a higher level of isotropy than both square and hexagonal lattice model. But one must use an interpolation procedure to relate the diagonal vectors to the corresponding nodes in choosing to connect a square grid with an octagonal streaming lattice. This quasi-nonlocal procedure may decrease the parallelizability of the model.

In our previous work,[11−13] an improved LBM which can simulate the incompressible Navier–Stokes equation was designed for both steady and unsteady flows. In this paper, we present a new incompressible model for MHD flows by introducing an additional lattice Boltzmann equation using magnetic distribution function to describe the evolution of the magnetic field. Compared with existing models, this model is more stable, usable, easily parallel-implemented and has higher accuracy. For the high Hartmann number, it simulates well. Especially, this incompressible model simulates well when the pressure gradient G is large while most of existing models would fail. The rest of the paper is organized as follows. In Section 2, the unified model is described in details. Then we will show how to use Chapman–Enskog expansion to recover the MHD equations in Section 3. Section 4 describes the use of the model to solve numerically the MHD problem of the Hartmann flow for several Hartmann numbers H, which parametrizes the solutions. We present the test simulations of the Hartmann flow in detail. There has been no detailed analysis about the problem ever before. We also make detailed comparison with Dellar's model. Section 5 concludes the paper.

2. Lattice Boltzmann MHD model

2.1. Lattice Boltzmann equation

The lattice Boltzmann equation describes the evolution of the particle distribution function f_i,

$$f_i(\boldsymbol{x} + c\boldsymbol{e}_i\Delta t, t + \Delta t) - f_i(\mathbf{x}, t) = \Omega_i. \tag{1}$$

For LBM, the LBGK single time relaxation method is often used for the collision term

$$\Omega_i = -\tau^{-1}\left(f_i(\boldsymbol{x}, t) - f_i^{\mathrm{eq}}(\boldsymbol{x}, t)\right), \tag{2}$$

where τ is the dimensionless relaxation time and f_i^{eq} is the equilibrium distribution function. It depends on the lattice and it is usually not uniquely defined. For lattices, the distribution function has the form given in Ref.[14]:

$$f_i^{\mathrm{eq}} = w_i\rho\left(1 + \frac{c\boldsymbol{e}_i\cdot\boldsymbol{u}}{c_s^2} + \frac{(c\boldsymbol{e}_i\cdot\boldsymbol{u})^2}{2c_s^4} - \frac{\boldsymbol{u}^2}{2c_s^2}\right), \tag{3}$$

where $\boldsymbol{e}_i$ is the discrete velocity direction, and $c = \dfrac{\Delta x}{\Delta t}$ is the particle speed, Δx, Δt, and τ are the lattice grid spacing, and the time step respectively. w_i are the weight coefficients such that $\sum\limits_{i\geq 0} w_i = 1$ and c_{s} is the sound speed, ρ is the density. They also depend on the lattice model. The commonly used lattice model is the DdQq given by Qian *et al*,[14] where d is the dimension and q is the number of the discrete velocity directions. For the D2Q9 lattice MHD model, we have $w_0 = \dfrac{4}{9}$, $w_i = \dfrac{1}{9}(i = 1-4)$, $w_i = \dfrac{1}{36}(i = 5-8)$, $c_{\mathrm{s}}^2 = \dfrac{c^2}{3}$. The velocity vectors, with magnitudes $|\boldsymbol{e}_i| = 1$ for $i = 1-4$ and $|\boldsymbol{e}_i| = \sqrt{2}$ for $i = 5-8$, form a square lattice, as illustrated in Fig.1.

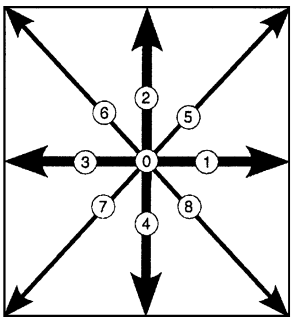


Fig.1. The nine particle speeds used by the hydrodynamic lattice Boltzmann equation.

2.2. Description of the incompressible MHD model

The incompressible MHD equations are

$$\nabla \cdot \boldsymbol{u} = 0, \tag{4}$$

$$\frac{\partial \boldsymbol{u}}{\partial t} + \nabla \cdot \left(p\boldsymbol{I} + \frac{\boldsymbol{B}^2}{2}\boldsymbol{I} + \boldsymbol{u}\boldsymbol{u} - \boldsymbol{B}\boldsymbol{B} \right) = \upsilon \nabla^2 \boldsymbol{u}, \tag{5}$$

$$\frac{\partial \boldsymbol{B}}{\partial t} + \nabla \cdot (\boldsymbol{u}\boldsymbol{B} - \boldsymbol{B}\boldsymbol{u}) = \eta \nabla^2 \boldsymbol{B}. \tag{6}$$

The magnetic field is solenoidial, $\nabla \cdot \boldsymbol{B} = 0$; and the fluid is incompressible, $\nabla \cdot \boldsymbol{u} = 0$. The two diffusion coefficients υ and η are the kinematic viscosity and magnetic resistivity, respectively. The relative importance of the viscous and resistive terms in the momentum and induction equations, respectively, is denoted by two dimensionless parameters, the Reynolds number $\mathrm{Re} = \dfrac{UL}{\upsilon}$ and magnetic Reynolds $\mathrm{Rm} = \dfrac{UL}{\eta}$, where U and L are velocity and length scales. It is well known that a small Mach number is equivalent to the incompressible limit. In this paper, we assume that two nonlinear terms $\boldsymbol{u}^2$ and $\boldsymbol{B}^2$ are comparable, in other words, that the fluid velocity is comparable with the magnetic field $B(O(\boldsymbol{u}) = O(\boldsymbol{B}) = O(M))$. Under the small Mach number limit, magnetic field and density variations are both $O(M^2)$.

The magnetic field is represented by a separate vector distribution function, which obeys a kinetic BGK-type evolution equation. Although there is no analogous microscopic process for the magnetic field, it can be argued that any conservative system can be formulated in this way under appropriate constraints. To derive the incompressible lattice model Eqs.(4–6), following the idea suggested in Ref.[15] we use two LBGK equations to solve the velocity and magnetic fields respectively:

$$\begin{aligned} &f_i(\boldsymbol{x} + c\boldsymbol{e}_i\Delta t, t + \Delta t) - f_i(\boldsymbol{x}, t) \\ =& -\tau^{-1}\left[f_i(\boldsymbol{x}, t) - f_i^{\mathrm{eq}}(\boldsymbol{x}, t)\right], \end{aligned} \tag{7}$$

$$\begin{aligned} &\boldsymbol{g}_j(\boldsymbol{x} + c\boldsymbol{e}_j\Delta t, t + \Delta t) - \boldsymbol{g}_j(\boldsymbol{x}, t) \\ =& -\tau_m^{-1}\left[\boldsymbol{g}_j(\boldsymbol{x}, t) - \boldsymbol{g}_j^{\mathrm{eq}}(\boldsymbol{x}, t)\right], \end{aligned} \tag{8}$$

where $\boldsymbol{e}_i$ or $\boldsymbol{e}_j$ is the discrete velocity direction. $f_i(\boldsymbol{x}, t)$ is the distribution function at node $\boldsymbol{x}$ and time t with velocity $c\boldsymbol{e}_i$, $f_i^{(\mathrm{eq})}(\boldsymbol{x}, t)$ is the corresponding equilibrium distribution depending on the lattice model used; $\boldsymbol{g}_j(\boldsymbol{x}, t)$ and $\boldsymbol{g}_j^{(\mathrm{eq})}(\boldsymbol{x}, t)$ are those of the magnetic field.

Remark 1 As mentioned in Refs.[15,16], we can use two independent LBGK models in Eq.(7) and Eq.(8), which depend on the lattice models and equilibrium distributions. For computational consistency and convenience, we use the same computational grid and particle speed for the two models; thus the set of discrete velocity directions in Eq.(8) is taken as the subset of those in Eq.(7).

The commonly used lattice model is the Bi-Stream model given by Martinez *et al*,[6] and compressible model given by Dellar.[7] Different from the common models, we take the pressure P as an independent variable in the equilibrium distribution as in Ref.[11] to derive a unified lattice MHD model $i\mathrm{D}d\mathrm{Q}q$. The velocity equilibrium distribution in $i\mathrm{D}d\mathrm{Q}q$ is defined as

$$f_0^{(\mathrm{eq})} = \rho_0 + \lambda_0 p - w_0 \times \frac{\boldsymbol{u}^2}{2c_{\mathrm{s}}^2} + (2w_0 - 1) \times \frac{\boldsymbol{B}^2}{2c_{\mathrm{s}}^2}, \tag{9}$$

$$\begin{aligned} f_i^{(\mathrm{eq})} =& \lambda_i p + w_i \left(\frac{c\boldsymbol{e}_i \cdot \boldsymbol{u}}{c_{\mathrm{s}}^2} + \frac{(c\boldsymbol{e}_i \cdot \boldsymbol{u})^2}{2c_{\mathrm{s}}^4} - \frac{\boldsymbol{u}^2}{2c_{\mathrm{s}}^2} \right. \\ &\left. + \frac{\boldsymbol{B}^2}{c_{\mathrm{s}}^2} - \frac{(c\boldsymbol{e}_i \cdot \boldsymbol{B})^2}{2c_{\mathrm{s}}^4} \right) \quad i > 0, \end{aligned} \tag{10}$$

where λ_i is the parameter defined by $\lambda_i = \dfrac{w_i}{c_{\mathrm{s}}^2}$, $\lambda_0 = -\sum\limits_{i>0} \dfrac{w_i}{c_{\mathrm{s}}^2} = \dfrac{w_0 - 1}{c_{\mathrm{s}}^2}$. w_i are the weight coefficients such that $w_i > 0$, $\sum w_i = 1$ and c_{s} is the sound speed. They depend on the lattice model. Constant ρ_0 is the mean density of flow.

$f_i^{(\mathrm{eq})}$ satisfies the following constraints:

$$\begin{aligned} &\sum_{i\geq 0} f_i^{(\mathrm{eq})} = \sum_{i\geq 0} f_i = \rho_0, \quad \sum_{i\geq 0} c\boldsymbol{e}_i f_i^{(\mathrm{eq})} = \boldsymbol{u}, \\ &\sum_{i\geq 0} c^2 \boldsymbol{e}_i \boldsymbol{e}_i f_i^{(\mathrm{eq})} = \left(p + \frac{\boldsymbol{B}^2}{2}\right)\boldsymbol{I} + \boldsymbol{u}\boldsymbol{u} - \boldsymbol{B}\boldsymbol{B}. \end{aligned} \tag{11}$$

The flow velocity, pressure, and kinematic viscous

are given by

$$\boldsymbol{u} = \sum_{i\geq 0} c\boldsymbol{e}_i f_i, \tag{12}$$

$$p = -\lambda_0^{-1}\left[\sum_{i\geq 0} f_i + s_0(\boldsymbol{u},\boldsymbol{B})\right] = \frac{c_{\rm s}^2}{1-w_0}\left[\sum_{i\geq 0} f_i + s_0(\boldsymbol{u},\boldsymbol{B})\right], \tag{13}$$

$$\upsilon = (\tau - 1/2)c_{\rm s}^2\Delta t, \tag{14}$$

where $s_0(\boldsymbol{u},\boldsymbol{B}) = -w_0\dfrac{\boldsymbol{u}^2}{2c_{\rm s}^2} + (2w_0-1)\dfrac{\boldsymbol{B}^2}{2c_{\rm s}^2}$.

For the iD2Q9 model, we have $w_0 = \dfrac{4}{9}$, $w_i = \dfrac{1}{9}(i = 1-4)$, $w_i = \dfrac{1}{36}(i = 5-8)$, $c_{\rm s}^2 = \dfrac{c^2}{3}$; for the iD3Q15 model, $c_{\rm s}^2 = \dfrac{c^2}{3}$, $w_0 = \dfrac{2}{9}$, $w_i = \dfrac{1}{9}(i = 1-6)$, $w_i = \dfrac{1}{72}(i = 7-14)$, and for the iD3Q19 model, $c_{\rm s}^2 = \dfrac{c^2}{3}$,$w_0 = \dfrac{1}{3}$, $w_i = \dfrac{1}{18}(i = 1-6)$, $w_i = \dfrac{1}{36}(i = 7-18)$.

To solve Eq.(6), we can use the same iDdQq lattice model used for magnetic field, and the equilibrium distribution $\boldsymbol{g}_i^{(\rm eq)}$ is taken as

$$\boldsymbol{g}_i^{(\rm eq)} = w_i\left(\boldsymbol{B} + \frac{1}{c_{\rm s}^2}c\boldsymbol{e}_i\cdot(\boldsymbol{u}\boldsymbol{B} - \boldsymbol{B}\boldsymbol{u})\right), \quad i \geq 0, \tag{15}$$

and

$$\sum_{i\geq 0}\boldsymbol{g}_i^{(\rm eq)} = \sum_{i\geq 0}\boldsymbol{g}_i = \boldsymbol{B},$$
$$\sum_{i\geq 0} c\boldsymbol{e}_i\boldsymbol{g}_i^{(\rm eq)} = \boldsymbol{B}\boldsymbol{u} - \boldsymbol{u}\boldsymbol{B}, \tag{16}$$

where w_i and $c_{\rm s}$ are the same as in the Eq.(7), as η in Eq.(6) is calculated by:

$$\eta = \left(\tau_{\rm m} - \frac{1}{2}\right)c_{\rm s}^2\Delta t. \tag{17}$$

As mentioned in the remark above, other lattice MHD models can be used for Eq.(6). For instance, Ref.[15] used iD2Q4 and iD2Q5 for Eq.(6) in 2D respectively. In general, we can also use iDdQ$(2d)$ or iDdQ$(2d+1)$ lattice for Eq.(6), and now $\boldsymbol{g}_i^{(\rm eq)}$ is taken as

$$\boldsymbol{g}_i^{(\rm eq)} = \frac{1}{b}\left(\boldsymbol{B} + \frac{b}{2c}\boldsymbol{e}_i\cdot(\boldsymbol{u}\boldsymbol{B} - B\boldsymbol{u})\right) \quad i \geq 0, \tag{18}$$

and η in Eq.(6) is calculated by:

$$\eta = \frac{1}{b}\times 2c^2(\tau_{\rm m} - 1/2)\Delta t, \tag{19}$$

where $b = 2d$ or $b = 2d+1$, corresponding to iDdQ$(2d)$ or iDdQ$(2d+1)$ lattice. $\boldsymbol{g}_i^{(\rm eq)}(\boldsymbol{x},t)$ defined by Eq.(18) satisfies the first two constraints in Eq.(16) and $\sum_{i\geq 0} c^2\boldsymbol{e}_i\boldsymbol{e}_i\boldsymbol{g}_i^{(\rm eq)} = \dfrac{1}{b}\times 2c^2\boldsymbol{B}\boldsymbol{I}$. iDdQ$(2d)$ consists of only the directions along axes, while iDdQ$(2d+1)$ the directions along axes and zero one. It is notable that $2d$ is the least number of discrete velocity directions. Similarly, following Ref.[15], through multi-scaling expansion, Eq.(6) can be derived to the second order from Eqs.(15) and (17), or Eqs.(18) and (19), under the low Mach number limitation.

Remark 2 Compared with the Dellar model[7] and most of traditional LBM models,[4−6,8] we substitute the pressure P for the density ρ in the equilibrium distribution functions just like Guo *et al* did in the Ref.[11]. With the new equilibrium distribution functions, we can recover the incompressible Navier–Stokes equations exactly without some higher order terms which may bring an undesirable compressible effect. Another main advantage is that our model can be more usable in dealing with external force. To drive the flow, firstly we can use the pressure difference between inlet and outlet, which is easily implemented in program. Secondly, we can add the general external force term to the right side of the evolvement equation as in Ref.[17]. Thirdly, we also can append factitiously external force into the equilibrium distribution function as Dellar did in Ref.[7]. However, there is a strict limitation in the Dellar method of handling external force. It is applicable only when the external force is constant.

2.3. Boundary condition

Most of the existing boundary schemes commonly used in LBM usually encounter numerical instability for flows at large Reynolds number. In a previous study, Guo *et al* developed in Ref.[16,17] a non-equilibrium extrapolation rule for velocity and pressure boundary condition, which is of second order with simple form and exhibits much better numerical stability. This rule is based on the decomposition of distribution function

$$f_i(\boldsymbol{x}_{\rm b},t) = f_i^{(\rm eq)}(\boldsymbol{x}_{\rm b},t) + f_i^{(\rm neq)}(\boldsymbol{x}_{\rm b},t), \tag{20}$$

where $f_i^{(\rm neq)}$ is the non-equilibrium part of f_i, $x_{\rm b}$ is a node on boundary.

For velocity boundary, we have

$$f_i(\boldsymbol{x}_{\rm b},t) = \overline{f}_i^{(\rm eq)}(\boldsymbol{x}_{\rm b},t) + (f_i(\boldsymbol{x}_{\rm f},t) - f_i^{(\rm eq)}(\boldsymbol{x}_{\rm f},t)), \tag{21}$$

while for pressure boundary, we use

$$f_i(\boldsymbol{x}_{\rm b},t) = \overline{\overline{f}}_i^{(\rm eq)}(\boldsymbol{x}_{\rm b},t) + (f_i(\boldsymbol{x}_{\rm f},t) - f_i^{(\rm eq)}(\boldsymbol{x}_{\rm f},t)), \tag{22}$$

where

$$\overline{f}_i^{(\mathrm{eq})}(\boldsymbol{x}_\mathrm{b},t)=\lambda_i p(\boldsymbol{x}_\mathrm{f},t)+s_i(\boldsymbol{u}(\boldsymbol{x}_\mathrm{b},t),\boldsymbol{B}(\boldsymbol{x}_\mathrm{b},t)), \quad (23)$$

$$\overline{\overline{f}}_i^{(\mathrm{eq})}(\boldsymbol{x}_\mathrm{b},t)=\lambda_i p(\boldsymbol{x}_\mathrm{b},t)+s_i(\boldsymbol{u}(\boldsymbol{x}_\mathrm{f},t),\boldsymbol{B}(\boldsymbol{x}_\mathrm{f},t)), \quad (24)$$

$\boldsymbol{x}_\mathrm{f}$ is the inner fluid node adjacent to $\boldsymbol{x}_\mathrm{b}$.

The same boundary treatment can also be applied on the magnetic field.

3. Derivation of the model equations

In this section we examine in detail the structure of the present model from the perspective of the Chapman–Enskog expansion procedure. Here we treat the long wavelength, low frequency behaviour of the system, including corrections to the ideal equations in the form of dissipative transport effects. We start from the discrete kinetic Eqs.(7) and (8) and expand up to the second order in time and space variables to obtain

$$\begin{aligned}&\Delta t D_i f_i(\boldsymbol{x},t)+\frac{(\Delta t)^2}{2!}D_i^2 f_i(\boldsymbol{x},t)\\ =&-\tau^{-1}\left(f_i(\boldsymbol{x},t)-f_i^{(\mathrm{eq})}(\boldsymbol{x},t)\right),\end{aligned} \quad (25)$$

$$\begin{aligned}&\Delta t D_i \boldsymbol{g}_i(\boldsymbol{x},t)+\frac{(\Delta t)^2}{2!}D_i^2 \boldsymbol{g}_i(\boldsymbol{x},t)\\ =&-\tau_\mathrm{m}^{-1}\left(\boldsymbol{g}_i(\boldsymbol{x},t)-\boldsymbol{g}_i^{(\mathrm{eq})}(\boldsymbol{x},t)\right),\end{aligned} \quad (26)$$

where $D_i=\partial t+ce_i\cdot\nabla$. Now we adopt the following multiple scale expansion. The time derivation, space derivation and particle distribution are expanded as

$$\partial t=\varepsilon\partial t_1+\varepsilon^2\partial t_2, \quad (27)$$

$$\nabla=\varepsilon\nabla_\gamma, \quad (28)$$

$$f_i=f_i^{(0)}+\varepsilon f_i^{(1)}+\varepsilon^2 f_i^{(2)}+\cdots, \quad (29)$$

where $f_i^{(0)}=f_i^{(\mathrm{eq})}$, $\boldsymbol{g}_i^{(0)}=\boldsymbol{g}_i^{(\mathrm{eq})}$ and the expansion parameter ε is assumed small, implying that t_2 has a slower time scale than t_1, and will be associated with diffusion effects. Since we are considering only one space scale, to simplify the notation in what follows, we will simply refer to ∇ (instead of ∇_γ). The expansion parameter will be retained to keep contributions of the same order. For particle distribution, we assumed the higher term of ε to small departure from equilibrium. Finally, the collision operator $\Omega_i=-\tau^{-1}\left(f_i(\boldsymbol{x},t)-f_i^{(\mathrm{eq})}(\boldsymbol{x},t)\right)$ can be written as $\Omega_i=-\tau^{-1}\left(\varepsilon f_i^{(1)}+\varepsilon^2 f_i^{(2)}\right)$.

Replacing all the expansions into Eqs.(25) and (26), we obtained

$$\varepsilon: \quad D_{1i}f_i^{(0)}=-\frac{1}{\tau\Delta t}f_i^{(1)}, \quad (30)$$

$$D_{1i}\boldsymbol{g}_i^{(0)}=-\frac{1}{\tau_\mathrm{m}\Delta t}\boldsymbol{g}_i^{(1)}, \quad (31)$$

$$\varepsilon^2: \quad \partial t_2 f_i^{(0)}+\frac{\Delta t}{2}D_{1i}^2 f_i^{(0)}+D_{1i}f_i^{(1)}=-\frac{1}{\tau\Delta t}f_i^{(2)}, \quad (32)$$

$$\partial t_2 \boldsymbol{g}_i^{(0)}+\frac{\Delta t}{2}D_{1i}^2 \boldsymbol{g}_i^{(0)}+D_{1i}\boldsymbol{g}_i^{(1)}=-\frac{1}{\tau_\mathrm{m}\Delta t}\boldsymbol{g}_i^{(2)}, \quad (33)$$

where $D_{1i}=\partial t_1+ce_i\cdot\nabla_\gamma$.

After algebraic manipulations the Eqs. (32,33) can be rewritten as

$$\partial t_2 f_i^{(0)}+\left(1-\frac{1}{2\tau}\right)D_{1i}f_i^{(1)}=-\frac{1}{\tau\Delta t}f_i^{(2)}, \quad (34)$$

$$\partial t_2 \boldsymbol{g}_i^{(0)}+\left(1-\frac{1}{2\tau}\right)D_{1i}\boldsymbol{g}_i^{(1)}=-\frac{1}{\tau_\mathrm{m}\Delta t}\boldsymbol{g}_i^{(2)}. \quad (35)$$

Multiplying Eqs.(30) and (31) and Eqs.(34) and (35) by 1 and ce_i, respectively, and summing over i, we get:

$$\nabla_\gamma\cdot\boldsymbol{u}=0, \quad (36)$$

$$\partial t_1\boldsymbol{u}+\nabla_\gamma\cdot\Pi^{(0)}=0, \quad (37)$$

$$\partial t_1\boldsymbol{B}+\nabla_\gamma\cdot\Lambda^{(0)}=0; \quad (38)$$

and

$$\partial t_2\boldsymbol{u}+\nabla_\gamma\cdot\Pi^{(1)}=0, \quad (39)$$

$$\partial t_2\boldsymbol{B}+\nabla_\gamma\cdot\Lambda^{(1)}=0; \quad (40)$$

where

$$\prod^{(1)}=\left(1-\frac{1}{2\tau}\right)\sum_{i\geq0}c^2\boldsymbol{e}_i\boldsymbol{e}_i f_i^{(1)}$$

and

$$\Lambda^{(1)}=\left(1-\frac{1}{2\tau}\right)\sum_{i\geq0}c\boldsymbol{e}_{i\alpha}\boldsymbol{g}_{i\beta}^{(1)}$$

$$\begin{aligned}\prod^{(1)}&=\left(1-\frac{1}{2\tau}\right)\sum_{i\geq0}c^2\boldsymbol{e}_i\boldsymbol{e}_i f_i^{(1)}\\ &=\left(\tau-\frac{1}{2}\right)\Delta t\sum_{i\geq0}c^2\boldsymbol{e}_i\boldsymbol{e}_i D_{1i}f_i^{(0)}\\ &=-\left(\tau-\frac{1}{2}\right)\Delta t\Big(\partial t_1\sum_{i\geq0}c^2\boldsymbol{e}_i\boldsymbol{e}_i f_i^{(0)}\\ &\quad+\nabla_\gamma\cdot\sum_{i\geq0}c^3\boldsymbol{e}_i\boldsymbol{e}_i\boldsymbol{e}_i f_i^{(0)}\Big)\\ &=-\left(\tau-\frac{1}{2}\right)\Delta t\left(\partial t_1\Pi^{(0)}+\nabla_\gamma\cdot\Gamma^{(0)}\right)\\ &\sim-c_\mathrm{s}^2\left(\tau-\frac{1}{2}\right)\Delta t\nabla^2\boldsymbol{u},\end{aligned} \quad (41)$$

$$\begin{aligned}\Gamma^{(0)} =&\sum_{i\geq 0} c^3 \boldsymbol{e}_{i\alpha}\boldsymbol{e}_{i\beta}\boldsymbol{e}_{i\gamma} f_i^{(0)}\\ =&c_{\rm s}^2(\boldsymbol{u}_\alpha\boldsymbol{\delta}_{\beta\gamma}+\boldsymbol{u}_\beta\boldsymbol{\delta}_{\alpha\gamma}+\boldsymbol{u}_\gamma\boldsymbol{\delta}_{\alpha\beta}),\end{aligned} \tag{42}$$

$$\begin{aligned}\Lambda^{(1)} =&\left(1-\frac{1}{2\tau_{\rm m}}\right)\sum_{i\geq 0} c\boldsymbol{e}_{i\alpha}\boldsymbol{g}_{i\beta}^{(1)}\\ =&-\left(\tau_{\rm m}-\frac{1}{2}\right)\Delta t\sum_{i\geq 0} c\boldsymbol{e}_{i\alpha}D_{i1}\boldsymbol{g}_{i\beta}^{(0)}\\ =&-\left(\tau_{\rm m}-\frac{1}{2}\right)\Delta t\left(\partial t_1\sum_{i\geq 0} c\boldsymbol{e}_{i\alpha}\boldsymbol{g}_{i\beta}^{(0)}\right.\\ &\left.+\nabla_\gamma\cdot\sum_{i\geq 0} c^2\boldsymbol{e}_{i\alpha}\boldsymbol{e}_{i\gamma}\boldsymbol{g}_{i\beta}^{(0)}\right)\\ =&-\left(\tau_{\rm m}-\frac{1}{2}\right)\Delta t(\partial t_1\Lambda^{(0)}+c_{\rm s}^2\nabla_\gamma\cdot\boldsymbol{B}_\beta\boldsymbol{\delta}_{\alpha\gamma})\\ \sim&-c_{\rm s}^2\left(\tau_{\rm m}-\frac{1}{2}\right)\Delta t\nabla^2\boldsymbol{B}.\end{aligned} \tag{43}$$

Combining the first order and second order terms, the MHD Eqs.(4–6) are derived to the order of $O(\varepsilon^2)(\varepsilon\sim\Delta t)$, $O(\varepsilon^2+\varepsilon M^2)$ and $O(\varepsilon^2+\varepsilon M^3)$ in continuity, momentum, and induction equation, respectively. They can be controlled by the parameter τ. The computation of p can be found in the Ref.[16] in details and the p also has a accuracy of order $O(\varepsilon^2+\varepsilon M^2)$ (with only one difference that $s_0(\boldsymbol{u},\boldsymbol{B})$ has two parameters.) The detailed process of calculation of $\Lambda^{(1)}$ and $\Pi^{(1)}$ is referred to Ref.[7].

4. Numerical simulation

Next, we apply our model to a linear magnetohydrodynamic problem named Hartmann flow.[18] This is the stationary flow of an incompressible, conductive fluid between two plates. Between the two plates, there is a homogenous magnetic field perpendicular to them. The direction of the initial magnetic field is chosen as the $y-$axis. We assume that the velocity of the fluid has only one component along the x-axis $\boldsymbol{u}=(u_x,u_y,u_z)=(0,0,0)$. The two plates are located at $y=L$ and $y=-L$. The flow produces an additional magnetic field. This field also has only an x component. The total magnetic field is $\boldsymbol{B}=(B_x,B_y,B_z)=(0,B_0,0)$, and $\rho=\rho(x)$, where B_0 is the constant strength of the initial magnetic field. From the continuity equation and the divergence-free condition of the magnetic field we get $\dfrac{\partial u_x}{\partial x}=0$ and $\dfrac{\partial B_x}{\partial x}=0$. Therefore, the nonlinear terms in the Navier–Stoke equation reduce to $(\boldsymbol{u}\cdot\nabla)\boldsymbol{u}=0$ and $(\boldsymbol{B}\cdot\nabla)\boldsymbol{B}=\left(B_0\dfrac{\partial B_x}{\partial y},0,0\right)$.

In the incompressible limit, the MHD equations for the Hartmann flow simplify to two linear equations:

$$\rho\nu\frac{\partial^2 u_x}{\partial y^2}+B_0\frac{\partial B_x}{\partial y}+G=0, \tag{44}$$

$$B_0\frac{\partial u_x}{\partial y}+\eta\frac{\partial^2 B_x}{\partial y^2}=0, \tag{45}$$

where G denotes a spatially uniform forcing in the along-channel direction, such as a pressure gradient. Assuming rigid and imperfectly conducting boundary conditions, so that both u_x and B_x vanish on $y=\pm L$, the Eqs.(44) and (45) has the exact solution

$$B_x(y)=\frac{\rho GL}{B_0}\left(\frac{\sinh(Hy/L)}{\sinh(H)}-\frac{y}{L}\right) \tag{46}$$

$$u_x(y)=\frac{GL}{B_0}\sqrt{\frac{\rho\eta}{\nu}}\coth(H)\left(1-\frac{\cosh(Hy/L)}{\cosh(H)}\right), \tag{47}$$

where $H=\dfrac{B_0L}{\sqrt{\rho\nu\eta}}$ is the Hartmann number that is the ratio between the magnetic and the viscous force. In the limit of zero Hartmann number without external field the solution reduces to $B_x=0$ and $u_x=\dfrac{(L^2-y^2)G}{2\rho\nu}$, which is the parabolic velocity profile of the Poiseuille flow. For large Hartmann numbers, the velocity profile is flattened. The velocity is almost constant between the two plates except in a thin boundary layer of thickness $\delta=\dfrac{L}{H}$, where the velocity rises from zero to the constant value $u_0=\dfrac{GL}{B_0}\sqrt{\dfrac{\rho\eta}{\nu}}$. The initial condition of the system was an equilibrium state with constant density $\rho=1.0$, pressures flow-in $p_{\rm in}$, flow-out $p_{\rm out}$ and a uniform magnetic field B_0 in the y direction. The velocity and the x component of the magnetic field was zero at the beginning of the simulation. The boundary conditions were realized by the method of non-equilibrium extrapolation.

It should be noted that the driven ingredient G in Eq.(44) can be realized through the pressure boundary condition, and we can also append an external force $F=G$ into the right side of Eq.(7) as in Ref.[15], while the external force F should satisfy some constraint. Additionally, we can append the external force F into the equilibrium equation as proposed by Dellar. We observed that simulations using above three different methods give results with very little difference.

Now we present the results of the simulation. The parameters used in the simulation are $\Delta x=0.02$, $\nu=\eta=0.01$, $p_{\rm in}=1.0016$, $p_{\rm out}=1.0$, $L=1.0$.

The lattice size is 8×100. To reach the steady state, a number of iterations are performed. The criterion of steady state is

$$\frac{\sum_{ij}\left|u_{ij}^{(n+1)}-u_{ij}^{(n)}\right|}{\sum_{ij}\left|u_{ij}^{(n+1)}\right|}\leq 3.0\times10^{-7},$$

where

$$u_{ij}^{(n)}=u(x_i,y_j,n\Delta t).$$

The flow is driven by a spatially uniform forcing in along-channel direction, such as a pressure gradient. We set it equal to $-G=\dfrac{1}{\rho}\times\dfrac{\partial(P+B^2/2)}{\partial x}$. In our simulation we set G=0.01,τ=0.95. Figure 2 shows the resulting velocity profiles and in Fig.3, the corresponding profile of the horizontal Magnetic field Bu is shown. The curves are the analytic solutions Eqs.(46) and (47). The simulation results agree well with the analytical solutions.

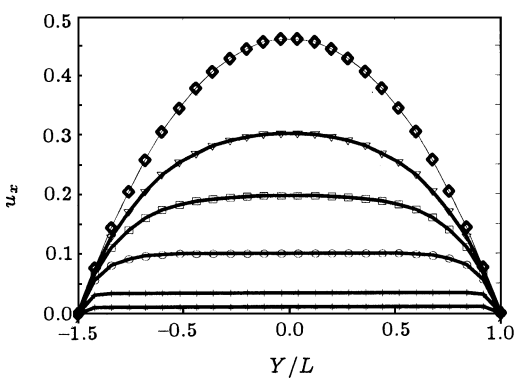


Fig.2. Profile of u (velocity in the x-direction) vs y/L for different Hartmann numbers: H=1 (diamonds), H=3 (triangles), H=5 (squares), H=10 (circles), H=30(pluses), H =100(stars). The solid lines are the theoretical results.

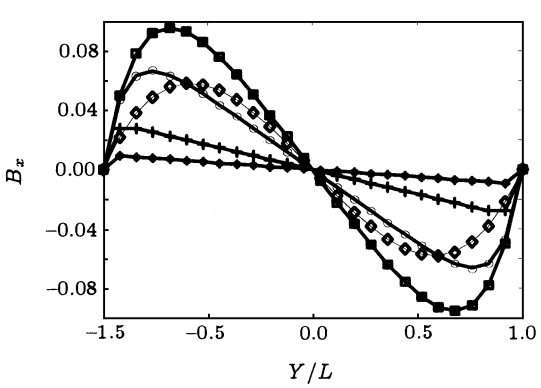


Fig.3. Horizontal magnetic-fields Bu vs y/L for different Hartmann numbers: H=1 (diamonds), H=5 (squares), H=10 (circles), H=30 (pluses), H=100 (stars). The solid lines are the theoretical results.

Figures 4 and 5 show that the parameters' relative global errors vary with the Hartmann number H and relax time τ, respectively. The Hartmann number $H=\dfrac{B_0L}{\sqrt{\upsilon\eta}}$ was varied by changing the magnitude of the magnetic field B_0. The kinematic viscosity υ and resistivity η can be obtained as a function of the relaxation time τ through Eqs.(14) and (17). In the past, the forcing coefficient G was usually set to 10^{-5} or even smaller to ensure that the distribution function f_i will only slightly depart from equilibrium during the evolvement process, while our model can simulate well when G was set to 0.1.

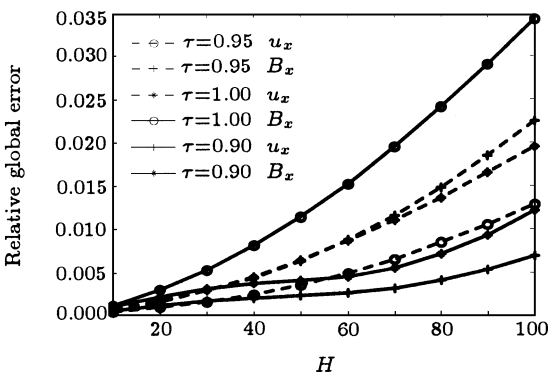


Fig.4. Hartmann number vs relative global error.

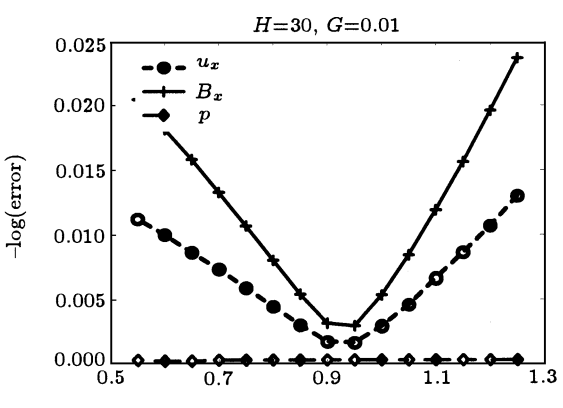


Fig.5. H=30. The relative global error also changes with relax time τ.

We have to take the Mach number $M\propto\Delta x$ to establish second-order convergence to the incompressible solution of Eqs.(46) and (47), since the incompressible error is $O(M^2)$ and the spatial truncation error is $O(\Delta x^2)$. The boundary condition of non-equilibrium extrapolation has also the second-order accuracy. Accuracy is evaluated by measuring the convergence rate of the relative global error as the lattice spacing varies, the relative global error is given

by

$$\|e(u)\|^2 = \frac{\sum_{ij}(u_{ij}^{(n)} - \overline{u}_{ij}^{(n)})^2}{\sum_{ij}(\overline{u}_{ij}^{(n)})^2},$$

where the summation is over the entire system, and $\overline{u}$ is the analytic solution given by Eq.(28). Also, we can get the relative global error of the horizontal component of magnetic fields. We use different lattice sizes 8×400, 8×200, 8×100 and 8×50 to simulate Hartmann flow. In Fig.6, the relative global errors are plotted logarithmically as functions of the lattice spacing. The slopes of the least-square fits are about 1.9936(u_x), 1.9821(B_x) and 1.9870(u_x), 1.9858 (B_x) for τ=0.95 and τ=1.1, respectively. It really shows the second-order accuracy. Compared with the existing compressible model[7] proposed by Dellar, our model has better stability and can be easily controlled by the above criterion of steady state while simulating.

In two dimensions, both the five-point lattice with weights $w_0 = \frac{1}{3}$, $w_i = \frac{1}{6}(i = 1-4)$ and the nine-point lattice with weights given above can be used on the magnetic field. In Figs.7 and 8, 5 symbolizes the five-point lattice while 9 symbolizes the nine-point lattice in the magnetic field. Through many tests, we found for the two models the results of five-point lattice had little difference with the nine-point lattice, and the difference is of the order 10^{-4}. As the evolvement time t grows, the relative global error of our model converges while the compressible model[7] diverges.

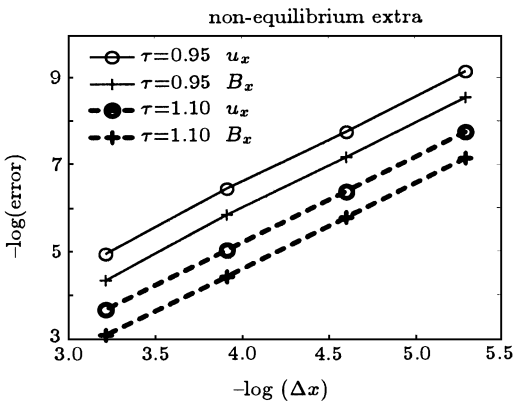


Fig.6. Relative global error for the Hartmann flow. The lines represent the least-squares fits. The slopes of the lines are: 1.9936 (u_x), 1.9821 (B_x), τ=0.95; 1.9870 (u_x), 1.9858 (B_x), τ=1.1, H=30.

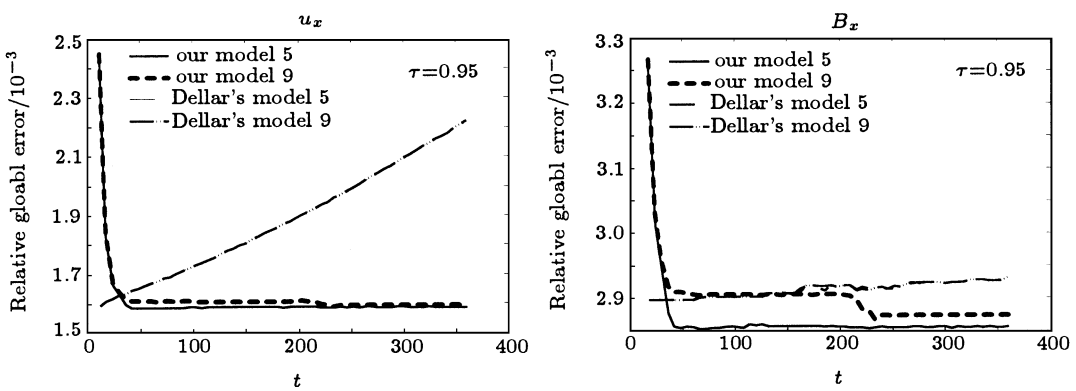


Fig.7. The convergence comparison of our incompressible model with Dellar compressible model. τ=0.95, H=30, G=0.01.

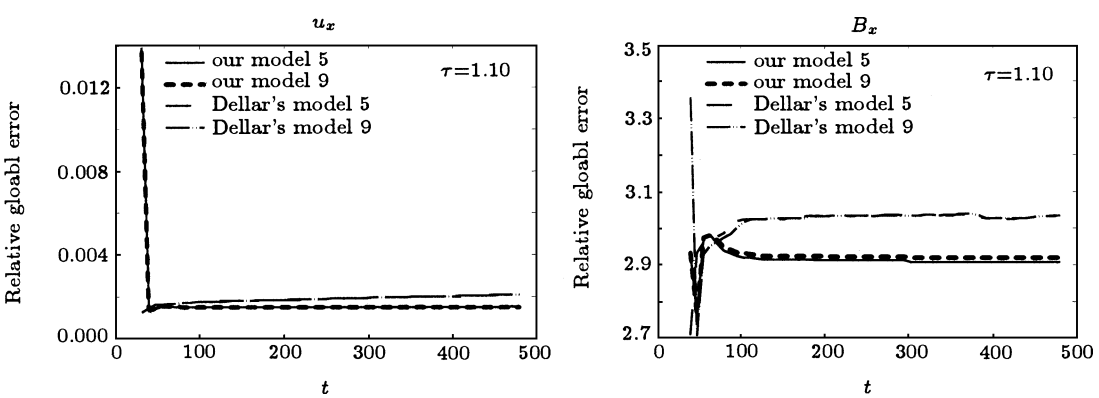


Fig.8. The convergence comparison of our incompressible model with Dellar's compressible model. τ=1.10, H=30, G=0.01.

Numerical results show that the velocity increases rapidly over a short distance from the boundary wall and decreases with the Hartmann number H growing, which well agrees with analytical solutions. The boundary layer, which has thickness $\delta \sim \left(\frac{\rho\nu}{\eta B^2}\right)^{1/2}$, is called the Hartmann layer. Then we found that $\frac{\delta}{L} \sim H^{-1}$. When $H \gg 1$, the thickness δ becomes very small and we need to increase the width of the domain to resolve δ. Therefore, if simulations with higher values of H are desired, L should be increased and the bigger sizes of lattice scheme are needed to round off the errors. This is not a limitation of the lattice Boltzmann simulation scheme, but rather a constraint because the computation of the analytic solution presents the same flaws.

5. Conclusion

In this paper, a new lattice Boltzmann incompressible MHD model is developed, which has an equilibrium distribution function in velocity different from Dellar.[7] Through multiscaling-expansion, the MHD equations are exactly recovered to the second order from the model. By choosing the distribution appropriately, the compressible effect is eliminated.

We apply the model to a linear problem (steady Hartmann flow) and it shows correct MHD behaviour. The simulation results using different parameters, such as the Hartmann number and the transport coefficients, have been presented for the test case previously considered in the literature, and compared with Dellar's solutions. Employing the non-equilibrium extrapolation boundary scheme, the method is of second order, has simple form and much better numerical stability. To drive the flow, we use the pressure difference between inlet and outlet. We can also add one controllable external force into the evolvement equation to realize it, which is referred in Ref.[17]. Another method is to add factitiously external force into the equilibrium distribution function as Dellar did in Ref.[7]. We simulated all of them. The results are the same, but the last one needs some space averages that may decrease the model's usability and is applicable only when external force is constant. Meanwhile, our model is independent of the density ρ whose variety during the evolvement process may lead to some undesired errors. Our model has more exactly take account of the incompressible condition $\nabla \cdot u = 0$ and eliminate some compressible effect brought by density term in earlier lattice Boltzmann MHD models.

Usually, the five-point lattice converges faster than nine-point lattice while the latter has better accuracy. But in our model, we observed that the five-point lattice converges faster and has the same accuracy or even better. Compared with the Dellar model,[7] our model is more stable and easily controlled. Although we have used the model to reproduce the Hartmann flow, future applications of the model to other complicated MHD flows are needed to show its usability. Application of the model extension to three-dimensional space is in progress.

Acknowledgments

We thank Professor Paul Dellar of Cambridge for having supplied us with his original LBE code that simulates the Hartmann flow and helpful discussions.

References

[1] Frisch U, Hasslacher B and Pomeau Y 1988 *Phys. Rev. Lett.* **61** 2332
[2] Montgomery D and Doolen G D 1987 *Complex Syst.* **1** 831
[3] Montgomery D and Doolen G D 1987 *Phys. Lett.* A **120** 229
[4] Chen H and Matthaeus W 1987 *Phys. Rev. Lett.* **58** 1845
[5] Chen H, Matthaeus W and Klein L 1988 *Phys. Fluids* **31** 1439
[6] Marinez D, Chen S and Matthaeus W 1994 *Phys. Plasmas* **1** 1850
[7] Dellar P 2002 *J. Comput. Phys.* **179** 95
[8] He X, Chen S and Doolen G D 1998 *J. Comput. Phys.* **146** 282
[9] Luo L S 2000 *Phys. Rev.* E **62** 4982
[10] Macnab A, Vahala G, Pavlo P, Vahala L and Soe M 2002 *Czechoslovak Journal of Physics.* **52** D59
[11] Guo Z L, Shi B C and Wang N C 2000 *J. Comput. Phys.* **165** 288
[12] He N Z, Wang N C and Shi B C 2004 *Chin. Phys.* **13** 40
[13] Zhou X Y, Shi B C and Wang N C 2004 *Chin. Phys.* **13** 712
[14] Qian Y H, Succi S and Orszag S A 1995 *Ann. Rev. Comp. Phys.* **3** 195
[15] Guo Z L, Shi B C and Zheng C G 2002 *Int. J. Numer. Meth. Fluids* **39** 325
[16] Guo Z L, Zheng C G and Shi B C 2002 *Chin. Phys.* **11** 366
[17] Guo Z L, Zheng C G and Shi B C 2002 *Phys. Rev.* E **65** 046308
[18] Ferraro V C A and Plumpton C 1961 *An Introduction to Magneto-Fluid Mechanics* (London: Oxford University Press) Chap. 2